Progress In Electromagnetics Research, Vol. 105, 49–69, 2010

PRACTICAL REMARKS ON MEASUREMENT AND SIMULATION METHODS TO EMULATE THE WIRELESS CHANNEL IN THE REVERBERATION CHAMBER

A. J. Pomianek, K. Staniec, and Z. Joskiewicz

Institute of Telecommunications, Teleinformatics and Acoustics
Wroclaw University of Technology
Wroclaw, Poland

Abstract—The purpose of this paper is to provide some further observations on the use of reverberation chambers to imitate real wireless channels. It is shown, that when RMS delay spread is calculated appropriate threshold has to be chosen. Based on the threshold value the required dynamics of measurements performed for realistic wireless channels can be estimated. It is also shown, that the reverberation chamber loading method allows only for representing outdoor channels.

1. INTRODUCTION

Currently, the utilization of wireless systems is rapidly growing. Thus in order to assure appropriate throughput, new methods for source and channel coding of the transferred data are under extensive development. However, in order to choose the most accurate scheme, a universal metric is required, the bit error rate (BER) being the most widely used. However, in order to obtain high-quality test results it is required to perform all the tests in a reliable and controllable environment, since BER is sensitive not only to the coding scheme but also to the changes of the wireless channel characteristics. In modern wideband wireless systems, apart from the received signal level also the time characteristic of the signal propagating in a given environment, plays an equally crucial role. Due to multiple signal reflections off the obstacles (a multipath phenomenon), decoders have to cope with receiving multiple copies of the transmitted signal. The basic measure of the multipath impact on wireless systems is the delay

Corresponding author: A. J. Pomianek (adam.pomianek@pwr.wroc.pl).

spread (τ_{RMS}), a factor which determines the maximum data rate achievable in the given propagation environment, without the need to use the channel equalization techniques. The importance of τ_{RMS} is not to be unappreciated, e.g., in CDMA cellular systems, where it is solely responsible for the loss of the signal orthogonality and thus is an indispensable component in the system performance formulas. As for other systems, a cyclic prefix has been deliberately added to OFDM symbol in WiMAX and WLAN 'a/g' systems to compensate for the effect of τ_{RMS}. Examples can also be cited where GSM communication has been disabled by excessive τ_{RMS} even despite sufficient received power level. Finally, the importance of the appropriate modeling of the delay spread has been demonstrated in COST 207 project which proposed reference models of τ_{RMS} using exponential profiles with one or two decaying peaks, discriminating between four terrain types: 1. urban, non-hilly, 2. rural, non-hilly, 3. bad urban, hilly and 4. hilly.

2. THEORY BEHIND THE TIME DELAY SPREAD

The analysis of the radio channels as a time-dispersive medium shall start with the observation that the emitted signal will propagate by interacting with the surrounding environment, that involves reflections from objects, transmissions thru obstacles, diffraction on edges and scattering from rough surface. Thus, the signal arriving at the receiver will not come in a single fringe, but as a pack of signals with different amplitudes, phases, angles of arrival, and short time delays, being delayed copies of the original signal. Once collected within a certain time span at a receiver, they sum up vectorially, accounting for their relative phase differences, which causes some copies to overlap constructively if both are in phase or cancel out otherwise. Such behavior leads to *small-scale fading*, which is a typical propagation effect, especially in the indoor and urban environment. Hence, the radio channel can be mathematically represented at any point in a three-dimensional space as a linear, time-variant filter (Fig. 1) of an

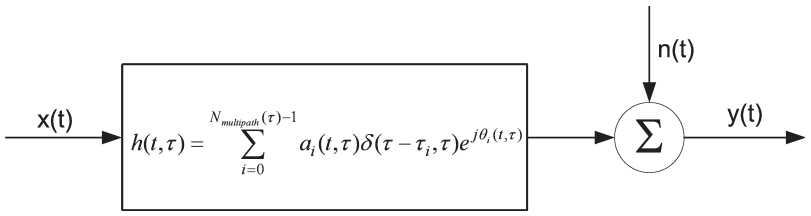

Figure 1. Wideband radio channel model.

impulse response given by (1a). The time variance appears here due to the temporal changes in real propagation environments, such as the motion of people, replacement of objects etc.

$$h(t,\tau) = \sum_{i=0}^{N_{multipath}(\tau)-1} a_i \delta(t-\tau_i,\tau) e^{j\theta_i(t,\tau)} \tag{1a}$$

$$H(f) = \int_{-\infty}^{\infty} h(t) e^{-j2\pi ft} dt \tag{1b}$$

In (1a), $h(t,\tau)$ is the radio channel impulse response, $N_{multipath}$ is the number of multipath components, $\theta_i(t)$ and $a_i(t)$ are respectively the time varying phase and amplitude of each component, and τ_i its delay. The frequency response $H(f)$ can be easily obtained from the Fourier transform of $h(t)$ (1b). Therefore, since either $h(t)$ or $H(f)$ are needed for an exhaustive characterization of the radio channel, only one of these should be measured (or accurately predicted), while the other one will be obtained by means of the Fourier transform or its inverse. Now, assuming that the signal is transmitted into an AWGN (Additive White Gaussian Noise) radio channel, the output signal will be in the form of (1c), where $x(t)$, $n(t)$ and $y(t)$ represent, respectively, the input signal, the channel white noise and the channel output signal.

$$y(t) = \int_{-\infty}^{\infty} x(\tau) h(\tau) d\tau + n(t) \tag{1c}$$

Crucial parameters with which to identify the characteristics of such a channel are: the mean excess delay τ_m, the root-mean square (rms) delay spread τ_{rms}, delay window, total energy, coherence (correlation) bandwidth $B_{x\%}(f)$ and the Power Delay Profile (PDP). The parameters of particular importance to PCS (Personal Communication Systems) systems design are PDP, τ_{rms}, $B_{x\%}(f)$. PDP represents the time distribution of the received signal power from a transmitted impulse, and is defined by (1d). It is often used to quantify time dispersion in mobile channels, and hence it characterizes the channel frequency selectivity. The mean excess delay τ_m is the averaged multipath delay (1e) and has the sense of the first moment of the PDP. Finally, τ_{rms}, having the sense of the second central moment of the PDP (1f), is a measure of the channel time dispersiveness and determines the maximum symbol rate achievable by a communication system before intersymbol interference (ISI) occurs (see also [12, 13]

for details).

$$P_h(t) = h(t)h^*(t) = |h(t)|^2 = \sum_{i=0}^{N_{multipath}-1} a_i^2 \delta(t-\tau_i) \tag{1d}$$

$$\tau_m = \frac{\sum\limits_i \tau_i P_h(\tau_i)}{\sum\limits_i P_h(\tau_i)} \tag{1e}$$

$$\tau_{rms} = \sqrt{\frac{\sum\limits_i (\tau_i - \tau_m)^2 P_h(\tau_i)}{\sum\limits_i P_h(\tau_i)}} \tag{1f}$$

As follows from literature [3, 4] BER is directly proportional to τ_{RMS}. The proportionality itself depends on the type of the assumed modulation. Thus, in order for measurements of new coding schemes to be viable, τ_{RMS} of the radio channel has to be strictly controlled during tests. This justifies the use of a dedicated test facility.

From the above discussion it stems to be essential to have an ability to effectively emulate wireless channel of various types. A well known test facility which possesses such ability is an electromagnetic reverberation chamber [1, 2]. In this paper some vital issues regarding the use of reverberation chamber for the purpose of imitating real propagation environments are discussed.

3. MEASUREMENTS

All measurements referred to herein have been conducted in the reverberation chamber of dimensions 7.78 m × 4.34 m × 3.10 m located at the Wroclaw University of Technology (WRUT) for the 2.4 GHz ISM band. The test setup is presented in Fig. 2. The EMCO 3111 horn and typical WLAN unipole have been used as the transmitting and receiving antenna, respectively. PDP was read directly from Agilent PNA-L N5230A vector network analyzer (VNA) with a built-in inverse FFT (IFFT) module. For IFFT calculations Kaiser windowing with $\beta = 6$ has been chosen. The IFFT was calculated from 6401 points of data collected with $IF = 150$ Hz. The VNA output power was fixed to +5 dBm. No smoothing and averaging were applied.

Since the properties of reverberation chambers are expected to be rather statistical then strictly stable, PDP was averaged over 25 distinct measurements, taken for successive stirrer (paddle) positions uniformly distributed over its full rotation and the PDP was normalized to its maximum power component. The results for an empty chamber

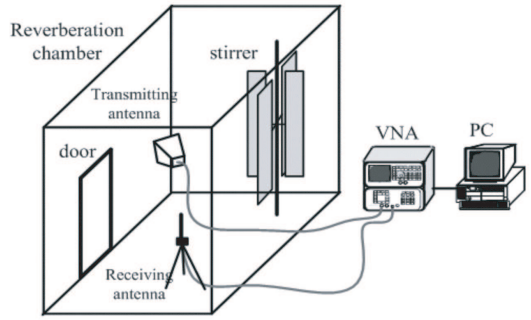

Figure 2. Illustration of test setup.

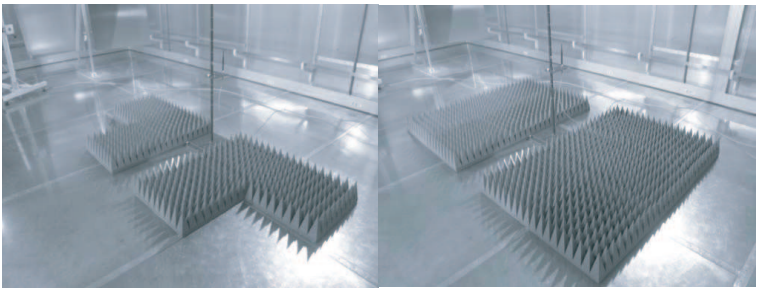

Figure 3. Arrangement of foam absorbers inside the reverberation chamber for 6 and 12 absorbers respectively.

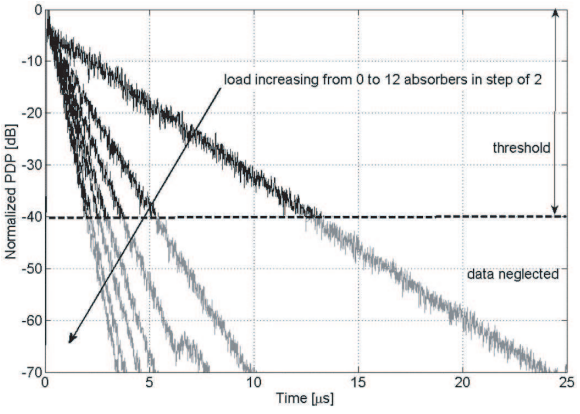

Figure 4. PDP achieved for different loads of reverberation chamber — Various number of foam absorbers inside the chamber.

as well as for the chamber loaded with a variable number of foam absorbers are shown in Fig. 4 which presents the shape of achieved normalized PDP with the dynamics truncated to the range of 70 dB. The arrangement of absorbers is shown in Fig. 3. In order to achieve τ_{RMS}, further calculations were performed in accordance with (1f).

4. CONTROLLING THE RMS DELAY SPREAD

Since the reverberation chamber is a large cavity resonator, in order to control τ_{RMS} (the measure of the effective time in which the energy is stored inside the cavity — a ring-down time), it suffices to control the power dissipation of the chamber/cavity [5]. The more load is applied to the chamber, e.g., in the form of microwave foam absorbers, the higher power dissipation occurs and the faster fades the power fed to the cavity. However, as follows from [6], in order to preserve the chamber reverberant properties, crucial for the channel emulation purposes, it cannot be overloaded. Therefore, the control of τ_{RMS} by changing the load of the reverberation chamber will allow for modification of τ_{RMS} in only a limited range. As the permissible loading of a chamber is hard to be strictly indicated [6] (the boundary is known, the required margin around is not), this method of managing the τ_{RMS} needs to be applied with caution, despite some works, e.g., [2] indicating that the chamber can be highly loaded during tests. From the above discussion stems a conclusion that some preliminary measurements of the loaded chamber properties are advisable before performing the target measurements of a particular coding scheme or a wireless system properties.

5. THRESHOLD FOR RMS DELAY SPREAD CALCULATIONS

Usually τ_{RMS} is extracted from a limited number of PDP components; those carrying power below a predefined threshold are neglected (see Fig. 4). This mechanism is commonly used in order to mitigate the impact of noise which is thereby rejected because its level lies below the threshold. It has been found that τ_{RMS} possesses an interesting inherent feature, which can be observed in Fig. 5. Namely, its value is not stabilized until some minimum dynamics has been assured (defined as the difference between maximum PDP component and the assumed threshold). It has been observed that τ_{RMS} remains invariant even if the threshold is further increased (note, that as follows from Fig. 4, noise floor is less than -70 dB). This indicates that the threshold level adjustment should not be set to the noise level, as is commonly

suggested. Instead, measurements of a real channel ought to be done with the use of methods assuring appropriate dynamics rather than an absolutely universal threshold (usually being the noise floor). Fig. 6 shows the difference between the RMS delay spread (obtained as a function of the threshold values) relative to the stabilized value of τ_{RMS} characteristic for various numbers of absorbers as a parameter. It appears that in order to keep this difference below 5%, a threshold

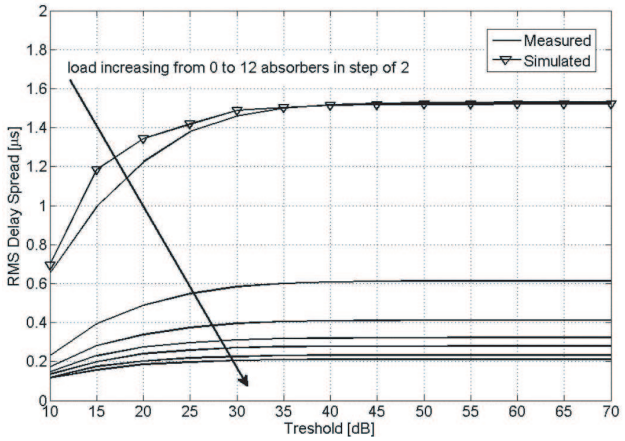

Figure 5. RMS delay spread calculated as a function of threshold relative to the maximum value of the PDP. For comparison a curve obtained in simulations is added.

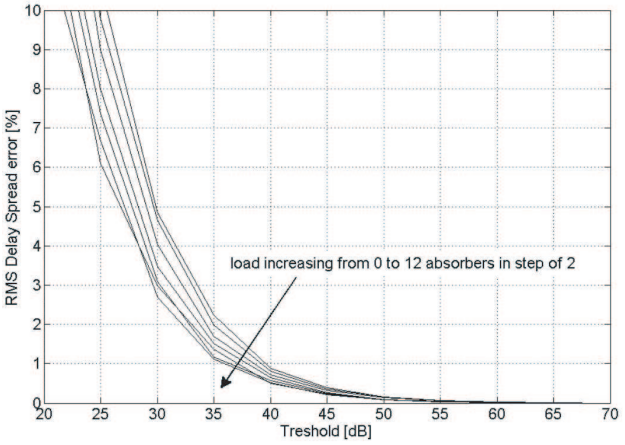

Figure 6. RMS delay spread percentage differences as a function of threshold relative to the maximum PDP component.

of at least 30 dB has to be maintained. This, in fact, means that for measurements of the real channel time characteristics to be correct, a separation of at least 30 dB of between peak PDP power component and the assumed threshold should be kept (Figs. 7 and 8). In order to keep the differences below 1%, at least 40 dB of separation is required. Smaller separation will results in deviations from the stable value τ_{RMS}. In practice, this is not a problem with a real reverberation chamber, since due to its excellent screening properties, the noise floor as low as −120 dB, whereas the dynamics of up to 70 dB can be easily obtained.

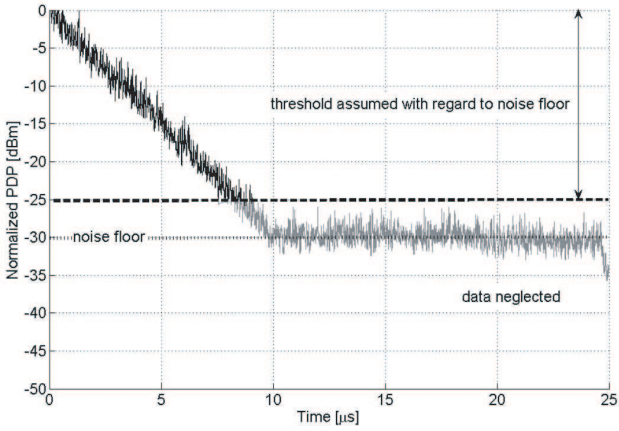

Figure 7. Unappropriate threshold level assumed with accordance to noise floor.

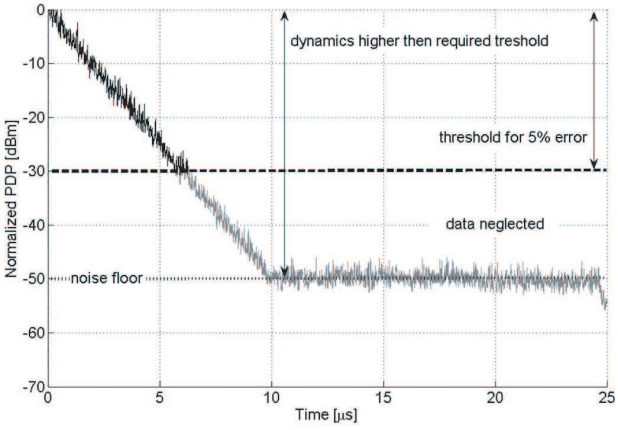

Figure 8. Correct threshold level assumed with accordance to error level. Appropriate dynamics assured.

6. RMS DELAY SPREAD AS A FUNCTION OF LOAD

The presented results are of minor importance when the channel emulation is the goal. For this purpose it is essential to know the dependency of achievable τ_{RMS} on the applied load. Such a dependency, represented by two groups of curves — A and B, is shown in Fig. 9. Group A consists of results from [1], their trend line and approximation given by (2). Group B presents the authors' results, their trend line and approximation given by (3). Both approximations are chosen so that the error does not exceed 5% on average (with respect to the respective trend line).

$$\tau_{RMS} = 0.277 \cdot A_{num}^{0.69} \tag{2}$$

$$\tau_{RMS} = 1.11 \cdot A_{num}^{0.69} \tag{3}$$

As (2) and (3) in which A_{num} stands for the number of loading absorbers, differ only by a scaling constant in the front, it appears that although the chambers and absorbers used in both experiments were different, the quantitative impact of increasing load on the achievable τ_{RMS} seems to follow a common formula (4). The absolute values of τ_{RMS}, however, are different.

$$\tau_{RMS} \sim A_{num}^{0.69} \tag{4}$$

This similarity seems to be partially explained by congruency of S_{11} parameter of both types of absorbers on one side, and by utilization of the same phenomenon (a loaded reverberation chamber) on the other side. The congruency of S_{11} parameter of both type of absorbers can be easily verified in [7] under the assumption that VHP-26-NRL absorbers were probably used in [1] whereas VHP-12-NRL were used by authors. Moreover, from results presented in Fig. 9 follows, that

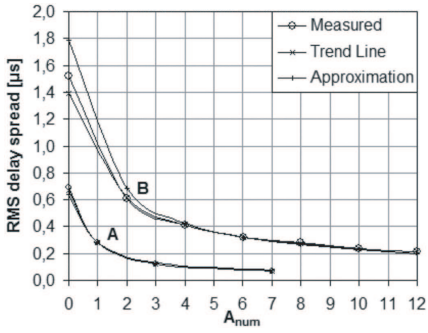

Figure 9. RMS delay spread as a function of load.

the larger chamber appears to be a better choice when a broader range of achievable τ_{RMS} is desired. More precisely: the smaller chamber in NIST (3.05 m × 4.57 m × 2.74 m) assures that τ_{RMS} in the range from 0.07µs up to 0.7µs will be achieved when loaded with, respectively, seven and no absorbers (empty chamber) [1]. The larger chamber in WRUT (7.78 m × 4.34 m × 3.10 m), in turn, assures achieving of τ_{RMS} in the range from 0.2 µs up to 1.6 µs when loaded with, respectively, 12 and unloaded (empty chamber). However, a larger chamber would probably require some additional mechanism other then absorber loading, when relatively small values of τ_{RMS} are to be achieved. Such a remark follows from Fig. 9, where it is well seen that increasing the load results in shortening the chamber response in terms of τ_{RMS} change with A_{num}. Particularly, from some point on the τ_{RMS} curve asymptotically approaches 0.2 µs which seems to be the boundary value. Such a behavior follows from two reasons: in an overloaded chamber only the direct component of the E-field reaches the receiving antenna (scattered components of E-field are considerably attenuated); the direct E-field component is not influenced by the chamber load, as the energy flow take place directly between the transmitting and receiving antennas (mainly due to the leakage of energy through the backlobes). Hence, when the chamber starts to be overloaded, τ_{RMS} will tend to the value resulting from PDP achieved for only the direct E-field component. To summarize this section, τ_{RMS} values resulting from measurements performed for various environments [8], as well as values achievable with the use of the reverberation chamber reported in [1] were assembled in Tab. 1. From the presented results it appears that both investigated reverberation chambers enable obtaining τ_{RMS} values that correspond to those obtained for outdoor rather then indoor propagation environments. This leads to the final conclusion that when the indoor propagation environment is to be emulated, i.e., such in which multipath propagation is the prevailing phenomenon, the chamber loading method will probably fail, even in smaller chambers. It is anticipated that lower values of τ_{RMS} may be expected by means of using an embedded chamber (a smaller chamber within the larger one). A verification of this hypothesis requires further analysis and measurements which are currently in progress.

It has to be remembered that only two different chambers were under consideration which may render some of the above remarks chamber-specific. Furthermore, as was already mentioned, in order to preserve the chamber reverberant properties crucial for the channel emulation purposes, the chamber cannot be overloaded. It is therefore of a great importance to obtain the delay spread curve (similar to those in Fig. 9) in preliminary measurements prior to the target performance

Table 1. RMS delay spread for various environments.

Environment	τ_{RMS} **[ns]**	**notes**
indoor at 850 MHz	270	max, office building [8]
indoor at 1500 MHz	$10 \div 50$	office building [8]
indoor at 1900 MHz	$70 \div 94$	office building [8]
urban at 910 MHz	$200 \div 310$	[8]
urban at 910 MHz	$1960 \div 2110$	extreme, [8]
loaded chamber	$70 \div 700$	[1]
loaded chamber	$200 \div 1600$	author's

measurements of a real coding scheme/wireless system. Unfortunately, it is not a trivial task. In order to verify whether the power distribution inside the loaded chamber obeys the Rayleigh distribution, a feature desirable during tests, it has to be directly measured. Such measurements are very demanding as regards the necessary time — these measurements are made on a point-by-point basis which is desired for mitigating the power distribution disturbances. From the authors' experience such a measurement campaign can take several working days, which justifies the use some CAD tools to expedite this analysis. The authors' team is currently developing a reverberation chamber simulator the use of which is supposed to allow potential investigators to efficiently increase the speed of analysis and thus the whole process of a wireless systems evaluation in multipath-challenged conditions. Since the simulator is a software tool, its speed can be further increased by the means of parallel computing. Additionally, the software unlike the real chamber, can be extensively utilized by several investigators simultaneously. Thus it is a more convenient and powerful approach then measurements in many instances.

7. REVERBERATION CHAMBER SIMULATOR

The deterministic model referred to in 6 is based on the Ray Launching technique; quite a vintage solution particularly applicable to indoor environments (not so fit for outdoors due to ray divergence problems). The software tool demonstrated herein is a variation of the model described in [9], customized for conditions present in the reverberation chamber. The basic principle consists in discretizing the transmitted wavefront into N angularly equidistant rays which number is given by (5), where $T \in (1, 2, 3, \dots)$.

$$N(T) = 10 \cdot 4^{T-1} + 2 \tag{5}$$

Such a procedure allows for an easy modeling of the Antenna Radiation Pattern as shown in Fig. 10 (keeping $T \geq 6$ for a stable gain in the modeled antenna [9]). Absorbers are modeled as parallelepiped blocks of almost ideally absorbing material ($0.6 \times 0.6 \times 0.2\,\mathrm{m}$ each).

With the simulator it is possible to track the discrete radio rays (each carrying a proportional part of the total radiated power, multiplied by the directional radiation characteristic) propagation inside the reverberation chamber until a maximum number of interactions has been achieved (set by the authors to 2750 due to the computer memory stack constraints) or until the power of the tracked ray has diminished below a level where its further contribution to the net received power is deemed negligible. An immediate advantage over measurements can be observed in Fig. 11. Instead of sampling the received E-field at distinct test points (as is usually the case with measurements unless a specialized, expensive array of probes is used) it is collected across the entire detection plane with resolution limited to individual 3D voxels volume (which size is commonly expressed in terms of the wavelength). Such a procedure, combined with the model's ability to record the exact spatial orientation (AoA — Angle-of-Arrival) and ToA (Time-of-Arrival) of each ray, allows for the collection of full information on the amplitude, angular and time characteristics of the signal propagating inside the reverberation

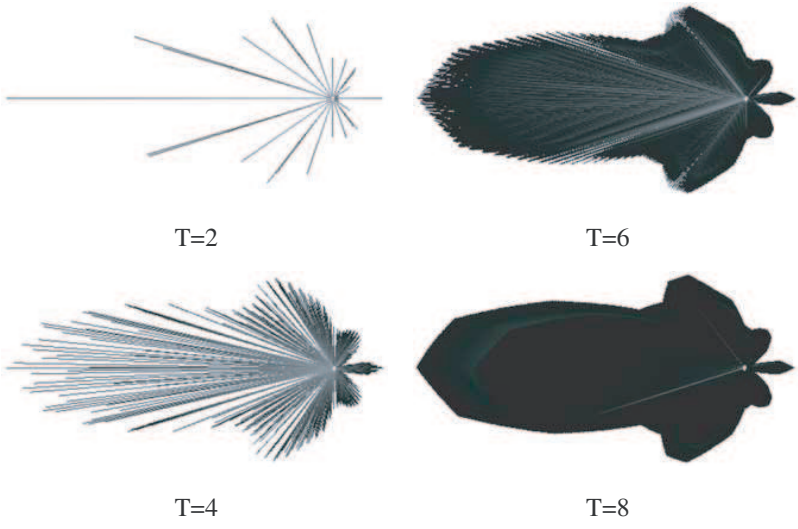

Figure 10. Discrete antenna ARP for different number of launched rays.

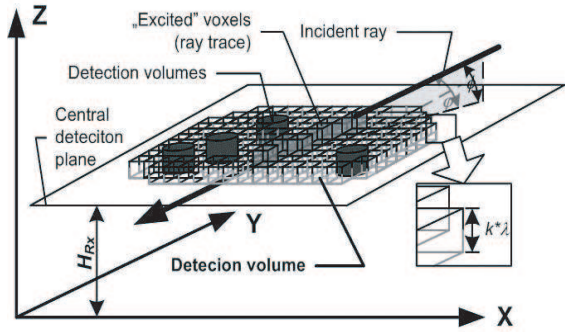

Figure 11. Information collection in voxels excited by the impinging wave.

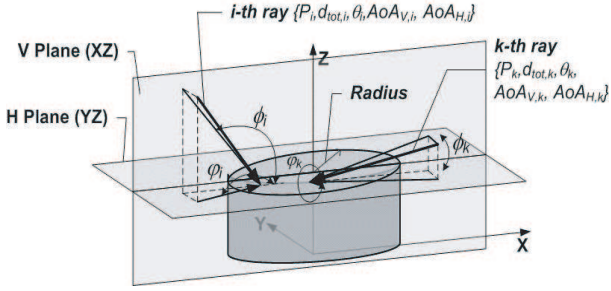

Figure 12. Angular data collection in a test point.

chamber. Fig. 12 demonstrates the information-gathering process in which an ith ray is described by a set of five parameters: amplitude (P_i), total distance traveled (d_{tot}), phase (θ_i) and AoA's in the vertical and horizontal planes ($AoA_{V,i}$ and $AoA_{H,i}$, respectively). Note that the same set of parameters is recommended in precise time channels analyses of IEEE 802.11 family systems (proposed in [11]).

The model presented here is in fact a customized version of another deterministic model originally intended for the prediction of power fading in indoor environments. The results of an extensive comparative campaign validating the model against propagation measurements was described in [9]. Some of the outcomes, selected in such a manner that they represent the model performance in extreme forms of the indoor environment, are shown in Figs. 13, 15. The cited environments are both located in the Department of Electronics at Wroclaw University of Technology (Poland): scenario 1 — a long corridor (111 m of length, Fig. 13) and scenario 2 — an arrangement of offices (20×21 m, Fig. 15).

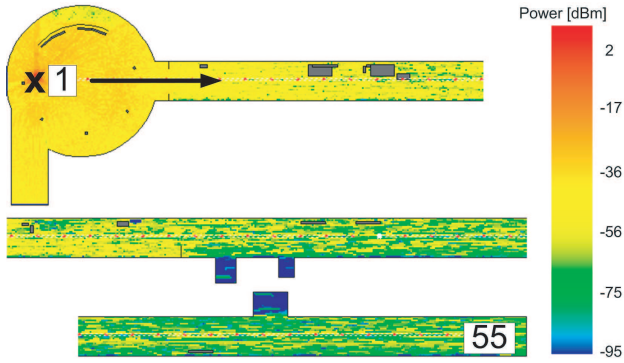

Figure 13. Simulated power distribution in scenario 1 (the long corridor, shown in three parts for visual ease).

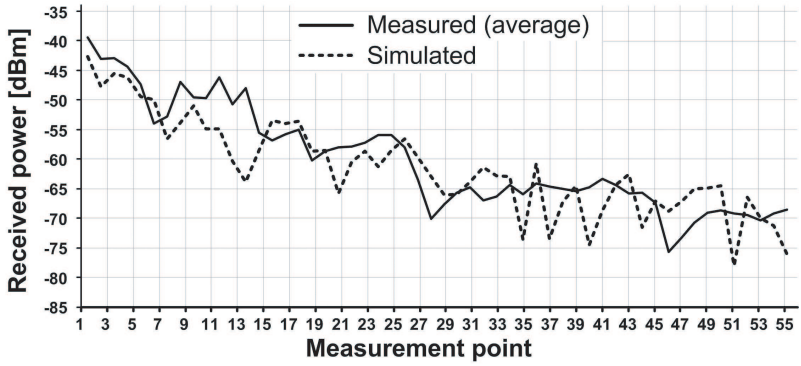

Figure 14. Comparison between measured and simulated power in scenario 1 (the long corridor).

In the propagation measurements the following equipment set-up was used:

- a directional transmit ISM antenna, 1.45 dBi at height of 1.5 m;
- a directional receive ISM antenna, 7.1 dBi at height of 1.3 m;
- a HP E4433B (ESG-D Series) Signal Generator, 250 kHz–4.0 GHz;
- a HP 8595E spectrum analyzer, 0–6 GHz;
- generator frequency setting: 2.45 GHz;
- generator power setting: 10 dBm.

In each environment a number of points were selected (red dots in Figs. 13, 15): 55 points in scenario 1 and 97 points in scenario 2.

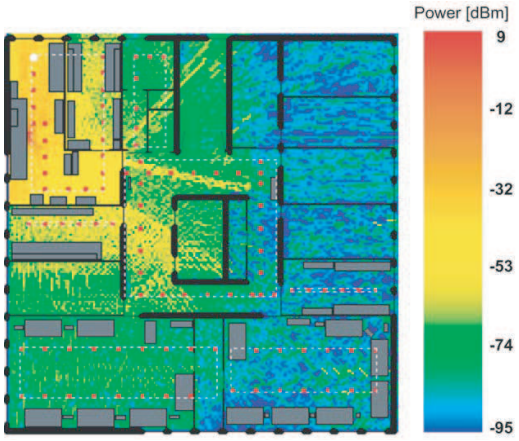

Figure 15. Simulated power distribution in scenario 2 (the office).

Next, four series of measurements were conducted in those points and averaged. The simulated power was also found at the very same points and compared with the averaged measured values. As can be seen in Figs. 14, 16 a good agreement was obtained in both aspects — that of absolute values in [dBm] and (even more important) the fading trend. The latter can be best observed in Fig. 16 where the transmitter was positioned in the left upper corner in scenario 2 while the receiver was moved all around the site — it is noteworthy that between points 29 and 65 the receiver was separated from the transmitter by an elevator shaft in the middle of the scene, mostly constructed of impenetrable materials, such as the reinforced concrete. Any signal reaching the receiver was thus transported by multiple reflections and diffractions to these points. The ability of the model to track such a behavior appears to be quite an encouraging proof of the model's validity; the mean square error calculated between the measured and simulated outcomes were found to be 7.1 dB and 5.5 dB for scenarios 1 and 2, respectively.

In the process of adapting the model to the specificity of propagation conditions inside the reverberation chamber, two factors turned out to be of an extreme importance in the simulated values of electric power and the signal time properties (the latter expressed in terms of the delay spread). Namely, the size of the receive probe and the walls reflectivity. Although the radiation patterns of the receive and transmit antennas were modeled accurately, it was not obvious what should be the appropriate dimension of the receive probe (one close to isotropic was used in measurements). It could be

conjectured that by augmenting the probe dimension (in other words, the active receive space) more rays would have the possibility to enter it thereby increasing the total power recorded by the probe. This assumption was proved correct in the course of experiments where the probe dimension (radius) was varied from 3 cm up to 7 cm — the resultant electric field averaged over the testfield changed by c.a. 10 dB (yielding 2.5 dB increase per 1 cm change in the probe size) — in the presented investigations the size of 3.5 cm was accepted yielding the closest results to those measured. As for the time delay spread, it remained almost perfectly constant (around 570 ns) regardless of the probe size. On the contrary to these results, as the wall reflectivity was varied within 0.0125–0.0525 dB, the received power changed by merely 1.5 dB whereas the time delay spread climbed exponentially from 236 up to 1098 ns. Lastly, as for the influence of the number of reflections considered, 100 reflections appeared to be just a sufficient number to obtain stable values of both received power and the time delay spread. These observations have lead to a remarkable conclusion that because the simulated power and τ_{RMS} respond oppositely, the determination of the optimal pair <probe size; wall reflectivity> reduces, in fact, to obtaining each pair component separately by tuning the model either to the measured power (sensitive to the probe size) or to the measured delay spread (sensitive to the wall reflectivity). Since in the authors' aim was to research the signal time properties, only the walls reflectivity Γ was therefore carefully tuned to meet the measured values of τ_{RMS} (in the unloaded-chamber case). Its final value equaled $\Gamma = 0.0085$ dB for the best-fit. A more in-depth analysis concerning the tuning of the deterministic model for the use in the reverberation chamber, is provided in [10].

As is common with all sorts of non-rigorous modeling methods, the model, after creation, needs to be tuned to measurements in order to find an operational point at which the program, under reference conditions, yields results comparable the measured. By so doing some degree of imperfection inherent to real-life measurements is "injected" into the otherwise idealized model. The procedure is in more depth described in [10] which concludes that the search of the operational point converges to finding a pair of tuning parameters: {1. the receiving probe radius; 2. the walls reflection loss}. Another handy observation in [10] is that the modeled amplitude and the time characteristics exhibit opposite behavior in response to changes in the tuning parameters. Utilizing this effect it is possible to find a best-for-all pair of parameters, each component found separately, namely the receiving probe radius by fitting the amplitude measurements; and the walls reflection loss by fitting the measured values of delay spread.

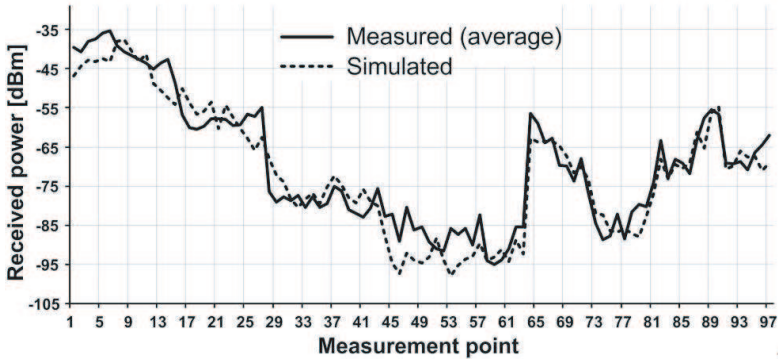

Figure 16. Comparison between measured and simulated power in scenario 2 (the office).

The conclusion in [10] regarding the influence of the assumed wall reflection loss (Γ) on τ_{RMS}, was based on the observation of the delay spread attained (in simulations) as a function of Γ. This situation is presented in Fig. 17 together with the best-fit curve plotted according to the estimate (6). An analogous figure of the simulated amplitude dependence of Γ is not cited in this paper since only the time aspects (τ_{RMS}) were the issue in investigations referred to in 3. Dependencies shown in Fig. 17 show that a 10-fold increase in the assumed wall reflection loss resulted in almost 5-fold decrease in the obtained delay spread. This clearly indicates that the tuning of the simulation algorithm to the measured results, in terms of selecting an appropriate value of Γ, is an indispensable procedure (in the current case the optimal value of Γ was found equal to 0,0085 dB per single reflection off the wall).

$$\tau_{RMS} = 32.058 \cdot \Gamma^{-0.665} \tag{6}$$

8. RESULTS OF INITIAL SIMULATIONS

In this section the authors will present results of numerous simulations in which the RMS delay spread (τ_{RMS}) was investigated as a function of the chamber loading (expressed in the number of absorbers). The outcomes presented herein were obtained by averaging τ_{RMS} over all 72 points located in the test field. To improve the statistical robustness even further, the averaging was also made over 51 stirrer rotations. Taking the advantage of the relatively short simulation time, the same calculations were performed for the absorbing panels modeled as "attached" to different walls. It was to verify whether

the reverberation chamber is responsive to the load positioning. The curves in Figs. 18 and 19 (each representing results for a different wall and frequency) show that some discrepancies do exist between τ_{RMS} obtained when different walls are loaded; up to 100 ns in difference for 2.45 GHz and up to 170 ns for 5.75 GHz. As can be noticed from direct comparison shown in Fig. 20, a good agreement between the simulated and measured results has been attained in terms of the initial (unloaded) value of τ_{RMS} (c.a. 1600 ns) and the final one — Achieved at the chamber overload threshold (c.a. 200 ns). As concerns the decreasing trend of τ_{RMS} as the number of absorbers rises, it also appears to be similar in the simulations and measurements although slightly more linear in the simulated case (Figs. 18 and 19) whereas more hyperbolical in the measured case (Fig. 4 curve B as well as Fig. 20).

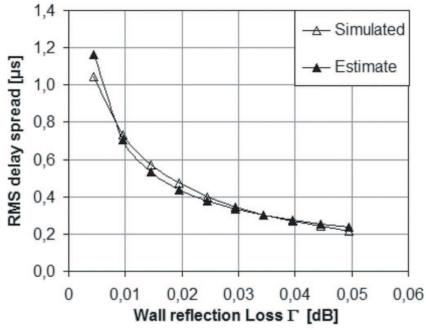

Figure 17. RMS delay spread dependence vs. assumed wall reflection losses.

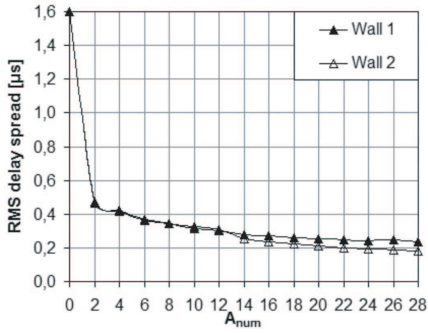

Figure 18. Simulated RMS delay spread as a function of load at the frequency of 2.45 GHz.

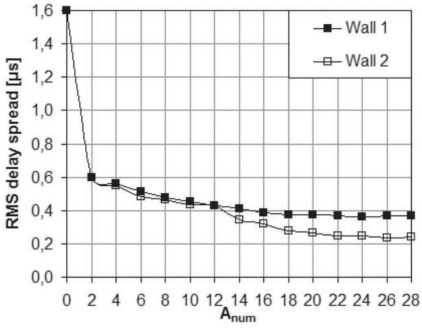

Figure 19. Simulated RMS delay spread as a function of load at the frequency of 5.75 GHz.

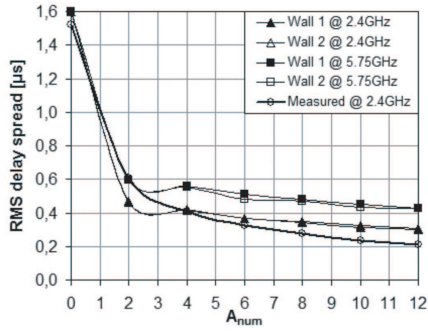

Figure 20. Simulated and measured RMS delay spread as a function of load.

It is somewhat surprising that despite averaging of the τ_{RMS} over all 72 test field points and 51 stirrer rotations, loading different walls yielded slightly different results. At this point it is hard to assess if observed discrepancies will have significant impact on the accuracy of coding scheme/wireless systems performance tests performed inside the chamber. What is still left to check is whether the same effect will be observed in measurements (the subjects has not yet been studied or at least unpublished in literature as for the authors' knowledge).

9. CONCLUSION

This paper has been devoted to some observations regarding the use of the reverberation chamber as a wireless channel emulator. It was shown that in order to stabilize the measured values of τ_{RMS} during measurements in a real wireless channel it is necessary to assure a minimum separation between the PDP peak power component and the peak noise power (e.g., $30 \div 40$ dB in the presented investigations). This indicates that upon a real channel RMS delay spread measurements the measurement method has to be carefully chosen with a particularly strong emphasis on its offered dynamics.

Moreover, for the purpose of a wireless channel emulation, the quantitative impact of the load applied to the chamber on τ_{RMS} has been determined to obey an approximate exponential relation (4). Nonetheless, in order for this dependency to be validated for chambers of different volume some further theoretical investigations are needed since the estimate (4) may turn out to hold true only for chambers very similar to those two presented in this paper.

It was proved by the means of measurements and simulations that the reverberation chamber-based emulator appears to provide an excellent test environment for outdoor rather then indoor channels, which statement seems to be independent on the chamber volume. This leads to a remark that the chamber loading method is insufficient when values of RMS delay spread typical for indoor propagation environment are to be obtained. Therefore, an alternative solution is required — possibly an embedded chamber (i.e., a small reverberation chamber inside a larger chamber) technique may be a solution. This however requires further analyses and measurements.

An alternative solution — in lieu of the time-consuming measurements — proposed by the authors is the use of a properly tuned reverberation chamber simulator. Some observations regarding such a simulator as well as its advantages have also discussed.

Further works will focus on several main aspects:

- validation of (4) for various arrangements of loading absorbers

inside the reverberation chamber
- defining the impact of embedding a smaller chamber, on PDP and RMS delay spread
- defining the impact of absorbers volume on the achievable RMS delay spread
- comparison of wireless systems performance for real and emulated outdoor channels

ACKNOWLEDGMENT

This paper has been written as a result of realization of the project "Next generation services and teleinformatics networks — technical, application and market aspects — electromagnetic compatibility". The contract for refinancing No. PBZ-MNiSW 02/II/2007.

REFERENCES

1. Genender, E., C. L. Holloway, K. A. Remley, J. Ladbury, G. Koepke, and H. Garbe, "Use of reverberation chamber to simulate the power delay profile of a wireless environment," *Proceedings IEEE EMC Europe*, Hamburg, Sep. 8–12, 2008.
2. Orlenius, C., M. Franzen, P. S. Kildal, and U. Carlberg, "Investigation of heavily loaded reverberation chamber for testing of wideband wireless units," *IEEE Int. Sym. on Antenna Propagation*, 3567–3572, Jul. 2006.
3. Saunders, S. R., *Antennas and Propagation for Wireless Communication Systems*, 2nd edition, John Wiley & Sons, 2007.
4. Chuang, J., "The effects of time delay spread on portable radio communications channels with digital modulation," *IEEE J. Selective Area on Cumm.*, Vol. 5, No. 5, 879–889, Jun. 1987.
5. Marcuvitz, N., *Waveguide Handbook*, Peter Peregrinus Ltd., 1993.
6. Holloway, C. L., D. A. Hill, J. M. Ladbury, and G. Koepke, "Requirements for an effective reverberation chamber: Unloaded or loaded," *IEEE Trans. on Electromagnetic Compatibility*, Vol. 48, No. 1, Feb. 2006.
7. Emmerson & Cumming, "Eccosorb VHP-NRL very high performance broadband pyramidal absorber," datasheet, www.Eccosorb.com.
8. Rappaport, T. S., *Wireless Communications: Principles and Practice*, 2nd edition, Prentice Hall, 2002.

9. Staniec, K., "The indoor radiowave propagation modelling in ISM bands for broadband wireless systems," Ph.D. Dissertation, Dept. Electronics, Wroclaw University of Technology, Wrocław, Poland, 2006.
10. Staniec, K., "Notes on the tuning of a deterministic propagation model in the reverberation chamber," *Proc. 2010 Asia-Pacific Symposium on Electromagnetic Compatibility & Technical Exhibition on EMC RF/Microwave Measurement & Instrumentation APEMC*, Beijing, China, in printed, Apr. 2010.
11. Erceg, V., et al., "TGn channel models," IEEE P802.11 Wireless LANz, May 2004.
12. ITU, ITU-R P.1145, Propagation data for the terrestrial land mobile service in the vhf and uhf bands.
13. ITU, ITU-R P.1407, Multipath propagation and parameterization of its characteristics.